ELSEVIER

Journal of Structural Geology 26 (2004) 1391–1400

JOURNAL OF STRUCTURAL GEOLOGY

www.elsevier.com/locate/jsg

Role of weak flaws in nucleation of shear zones: an experimental and theoretical study

Nibir Mandal, Santanu Misra, Susanta Kumar Samanta*

Department of Geological Sciences, Jadavpur University, Kolkata 700032, India

Received 14 April 2003; received in revised form 29 December 2003; accepted 5 January 2004

Available online 21 February 2004

Abstract

This paper investigates the role of inherent weak flaws in the formation of plastic zones in deforming solids to understand the development of geological shear zones. Physical experiments were carried out on polymethylmethaacrylate (PMMA) models containing single and multiple circular cylindrical flaws under compression, maintaining plane strain condition. Models with single flaws show development of shear zones against a flaw in the form of conjugate sets with an average dihedral angle of 84° and oriented at an angle of 42° to the bulk compression direction. The shear zones are generally tapered, with increasing width away from the flaw. In models with multiple flaws, shear zones nucleated against individual flaws, which propagated and coalesced with one another, forming through-going, band-like shear zones with inclination varying from 35° to 53° with the bulk compression direction. With an increase in flaw concentration, the through-going shear zones defined persistent conjugate sets. We applied the plane theory of elasticity for numerical simulations of ductile shear zones under the influence of a single circular weak flaw. The pattern of shear zones yielded from numerical runs grossly matches with those observed in physical model experiments. Theoretical analysis demonstrates that the presence of a flaw promotes nucleation of shear zones at a bulk stress below the yield strength of matrix. This critical stress is a non-linear function of the flaw–matrix competence contrast, and decreases asymptotically with increasing competence contrast.

Keywords: Stress; Yield strength; Plastic strain; Physical models; Theory of elasticity

1. Introduction

Many rocks contain inherent flaws in the form of inclusions, which perturb the strain field during deformation. A number of experimental and theoretical models have been applied to investigate the nature of strain perturbation in inclusion–matrix rock systems, and development of several geological structures, such as folialtion drag, porphyroblast trails, porphyroclast tails etc. (Masuda and Ando, 1988; Ildefonse and Mancktelow, 1993; Passchier, 1994; Bjornerud and Zhang, 1995; Kenkmann and Dresen, 1998; Jezek et al., 1999; Pennacchioni et al., 2000; Ramsay and Lisle, 2000; Treagus and Lan, 2000; Mandal et al., 2001). Apart from influencing the development of the aforesaid geological structures, the presence of any geometrical or mechanical imperfection within a rock body can also aid nucleation of high-strain zones (Tvergaard et al., 1981; Segall and Simpson, 1986). It has been shown that solid materials deformed under critical stresses develop high-strain zones in the form of plastic bands (Hill and Hutchison, 1975; Cobbold, 1977; Anand and Spitzig, 1980; Porier, 1980; Mandal et al., 1992; Mair et al., 2000), which are comparable with ductile shear zones observed in naturally deformed rocks. This is also evident from studies based on real rocks and rock analogue models, which demonstrate that mechanical heterogeneity in rock systems can lead to strain localization in the form of shear zones (Christiansen and Pollard, 1997; Grujic and Mancktelow, 1998; ten Grotenhuis et al., 2002). Recently, Mancktelow (2002) has presented finite element models for the development of conjugate shear zones in viscoelastic inclusion–matrix systems. The models demonstrate the influences of different physical factors, like power law rheology, strain softening, effective viscosity contrast between the inclusion and matrix, in the propagation behaviour and thereby the geometry of shear zones.

This study is based on physical experiments using

* Corresponding author. Tel.: +91-33-414-6214; fax: +91-33-856-0008.
E-mail address: susanta_ju@hotmail.com (S. Kumar Samanta).

0191-8141/$ - see front matter © 2004 Elsevier Ltd. All rights reserved.
doi:10.1016/j.jsg.2004.01.001

polymethylmethaacrylate (PMMA) models, and demonstrates the controls of weak flaws in plastic failure of the matrix material, leading to nucleation of shear zones. The experiments were run on models containing single as well as multiple flaws. The plane theory of elasticity is employed to determine the stress field around a flaw in an elastic–plastic material, and to simulate shear zones, imposing Von Mise's criterion for plastic failure in the neighbourhood of flaw. The bulk stress required for nucleation of shear zones is derived as a function of the competence contrast between the matrix and flaw.

2. Analogue models

2.1. Experimental methods

We ran deformation experiments on PMMA models There are several advantages in using PMMA for the present study. The material behaves plastically under atmospheric pressure and temperature conditions, and the onset of plastic deformation is evident macroscopically from the stress–strain curves (Fig. 1). The PMMA that we used is transparent and can be studied under an ordinary optical microscope in thin section. The polymer has a characteristic optical property, which has been utilized in our study. It is optically isotropic, but turns anisotropic as soon as it is plastically strained (Bowden and Raha, 1970; Anand and Spitzig, 1980). In addition, the birefringence increases with increasing plastic strain, giving a scope for assessing qualitatively the intensity of plastic strain by observing the degree of optical anisotropy. This strain-dependent optical property was used to study the localization of shear zones in the neighbourhood of inherent flaws.

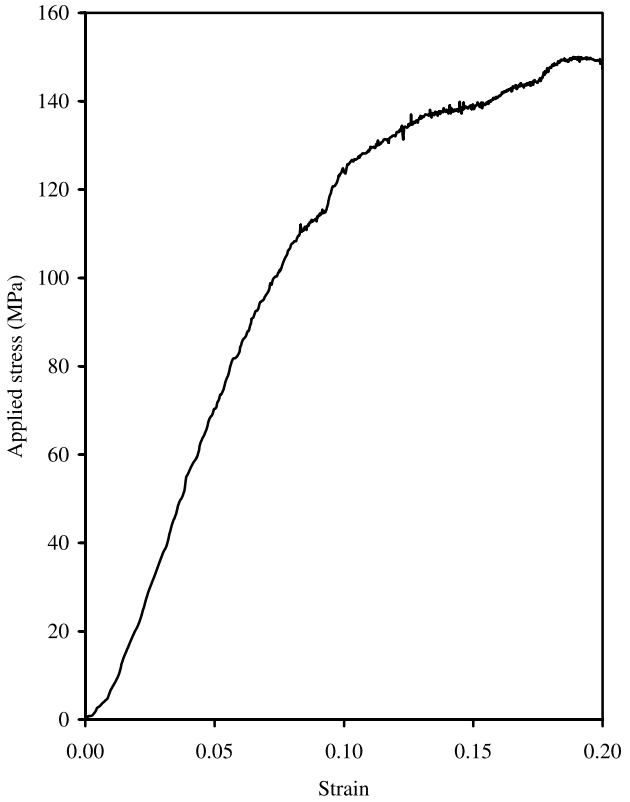

Fig. 1. Stress–strain relation for polymethylmethaacrylate (PMMA) obtained from deformation tests on homogeneous PMMA models.

PMMA models were prepared in the following manner. A number of plates of desired dimensions (6 cm × 4 cm) were cut out from a 1.1-cm-thick PMMA sheet, and the plates were then stacked with their interfaces welded with a strong adhesive to develop a single, thick block. In order to induce weak perturbations in the model, the block was drilled to make circular cylindrical holes, which were later filled with epoxy, a material much weaker than PMMA. The ratio of shear moduli of PMMA and epoxy is 9.21. The lateral faces of the block were finally polished to gain an exact dimension of the model required for placing it within the deformation zig (Fig. 2).

Model deformation was run under a hydraulically driven apparatus with arrangements for tracking the applied load and the displacement in the course of progressive deformation. The experiments were performed in plane strain, with the no-strain direction along the axes of flaws (Fig. 2), at strain rates in the order of $5 \times 10^{-4}\ s^{-1}$ and for a finite shortening up to a maximum of 22%. Deformed models were studied in both macro- and micro-scale. For macro-scale observations, square grids were marked on the lateral faces (perpendicular to flaw axis) of the model, and their distortion patterns revealed localization of shear zones in the neighbourhood of flaws. In order to study the deformed model under an optical microscope we prepared a single thin section from a slice of the model, cut transverse to the flaw axis. However, under the optical microscope it was difficult to take photographs of the overall dispositions of shear zones around a flaw in a single snap. We thus developed a special arrangement, which consisted of two polarising plates within a cylindrical tube, being illuminated from one side. The deformed specimen was placed within

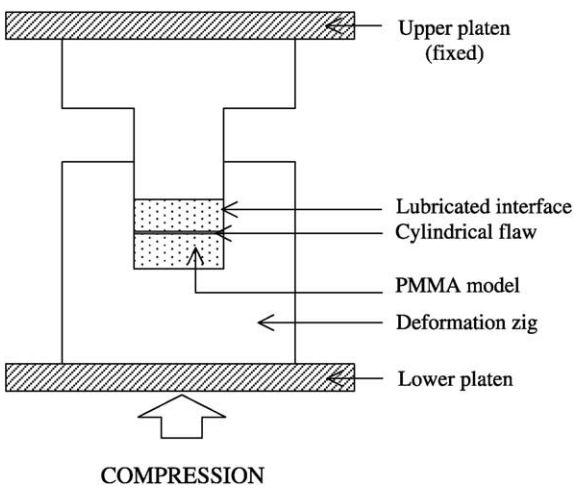

Fig. 2. Schematic sketch of experimental set-up for model deformation.

the polarising plates. The latter were rotated to a mutually crossed position. In this position the specimen became dark, revealing the shear zones in the form of birefringence domains. The overall patterns could be observed and photographed at a glance.

2.2. Experimental results

2.2.1. Models with single flaws

We carried out a set of experiments on PMMA models containing single flaws (Fig. 3a) During deformation, the flaws were flattened into elliptical cross-sections. The passive square grids in the neighbourhood of the flaws were intensely distorted in locales resembling shear zones (Fig. 4a). The strain distribution shows that the high-strain zones localize preferentially near the tips of the flattened flaws (Fig. 5), implying that the flaws act as the nucleation site of shear zones. Optical studies also reveal that the weak flaws acts as a site for nucleation of shear zones, showing strong birefringence (Fig. 4b). The shear zones occur as conjugate sets, radiating from the flaw. Individual shear zones show wedge shaped geometry, with increasing width away from the flaw (Fig. 4c). In order to express the shear zone orientation we constructed central lines of tapered shear zones, and measured their inclination. The dihedral angle of shear zones, on average, is estimated as 84°, where individual shear zones make an angle of 42° to the bulk compression direction. Their optically defined boundaries are sharp near the flaw, which become more and more diffuse away from the flaw. In addition, the intensity of optical anisotropy tends to be progressively weak, indicating that the overall strain within a zone also decreases away from the flaw (Fig. 4b), which is also reflected in the strain distribution obtained from the deformed grids (Fig. 5). This type of tapered geometry of shear zones is noticed in numerical models presented in the next section.

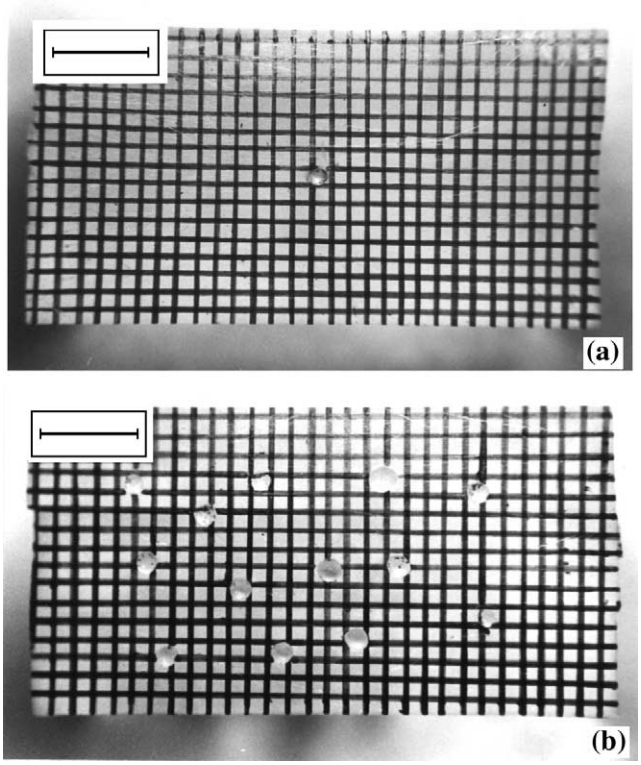

Fig. 3. Initial PMMA models containing (a) single and (b) multiple circular cylindrical flaws. Flaw axis is along the viewing direction. Scale bar: 1 cm.

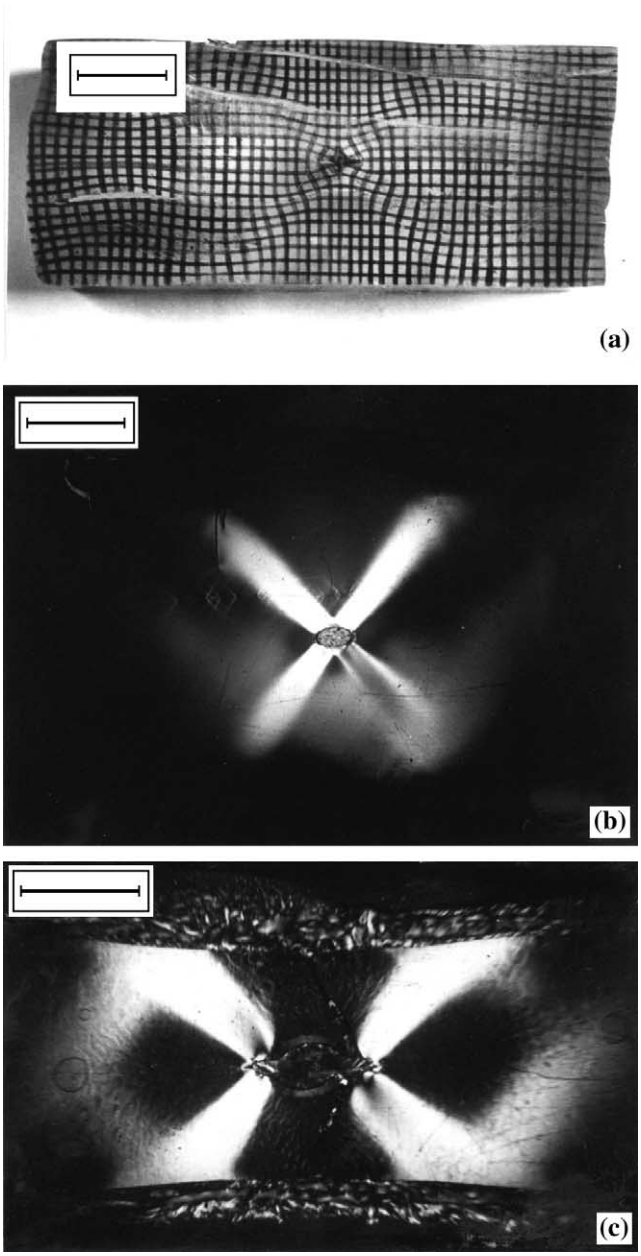

Fig. 4. PMMA models deformed under vertical compression. (a) Distortion of grids defining shear zones radiating from the flaw. Permanent bulk shortening in the model was 12%. Scale bar: 1 cm. (b) Overall disposition of shear zones (birefringence zones) in thin sections under cross-nicols. Permanent bulk shortening in the model was 5%. Scale bar: 1 cm. (c) Wedge shaped geometry of shear zones. Permanent bulk shortening in the model was 21%. Note that the shear zones appear to terminate abruptly at the plate boundary, as the photograph was taken after removing the lower and upper polymer plates of the deformed model. Scale bar: 0.5 cm. The three figures represent three different PMMA models.

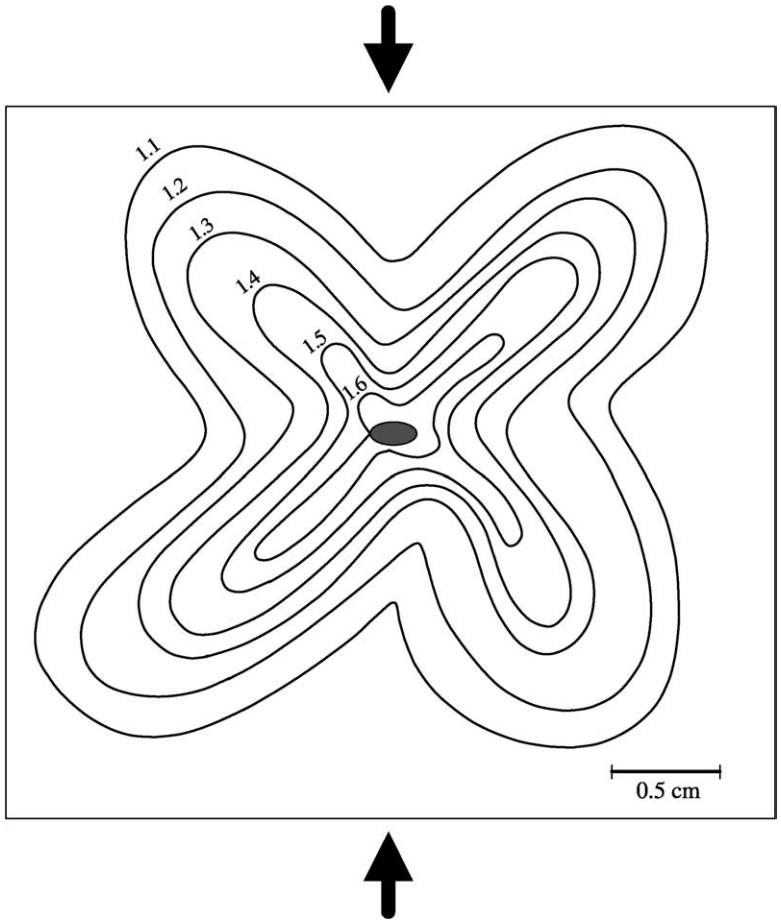

Fig. 5. Strain map around the flaw in deformed model shown in Fig. 4a. Numerical values corresponding to strain contours indicate the principal stretch.

The shear zones propagated to a large extent, and met the surface of the PMMA plate. Minor shear zones formed in the locales where the flaw-controlled shear zones met the surface of the model. These shear zones nucleated at the surface, and propagated inside and narrowed down to terminate in the central part of the models (Fig. 4c). These subsidiary shear zones are oriented at angle of 35° to the bulk compression direction, which is slightly less than that of dominant shear zones.

2.2.2. Models with multiple flaws

We performed a number of experiments on PMMA models containing multiple weak flaws (Fig. 3b). In contrast to single flaw models, these models show shear zones, nucleating against individual flaws, of diverse orientations, with inclinations to the bulk compression varying in a wide range (24°–59°). The shear zones coalesce with one another while propagating away from the flaws, and form longer *through-going shear zones* with an overall band-like geometry (Fig. 6). The experiments show that the development of shear zones is controlled by the distribution of flaws. They form in such a fashion that they link two neighbouring flaws, describing a maximum width at the central distance between the two flaws (Fig. 6a). The coalescence of two neighbouring shear zones appears to be more effective when the flaws are aligned along a line with orientation close to that of shear bands as observed in models with single flaws. Shear zones connecting two flaws do not form when the latter are aligned far away from this orientation.

When the flaw concentration is low, the models developed through-going shear zones non-uniformly, showing an association with discrete shear zones. In terms of orientation, however, the shear zones occur in conjugate sets. In contrast, models containing flaws in relatively large concentrations developed more persistent through-going shear zones in conjugate sets (Fig. 6b). This is probably due to the more effective coalescence of shear zones as a flaw arrangement of favourable orientations is more available in systems of densely distributed flaws. In multiple flaw models the general trend of through-going shear zones varies in the range from 35° to 53° with respect to the bulk compression direction (Fig. 6b).

In these experiments the shear bands in places show offsetting at the interfaces of two polymer plates. It appears that some slip occurred locally along the plate interfaces, resulting in offsetting of a shear band across the interface. The slip probably developed at locales where the adhesive material was not properly spread on the surface of the plate during model preparation. This is a limitation in our

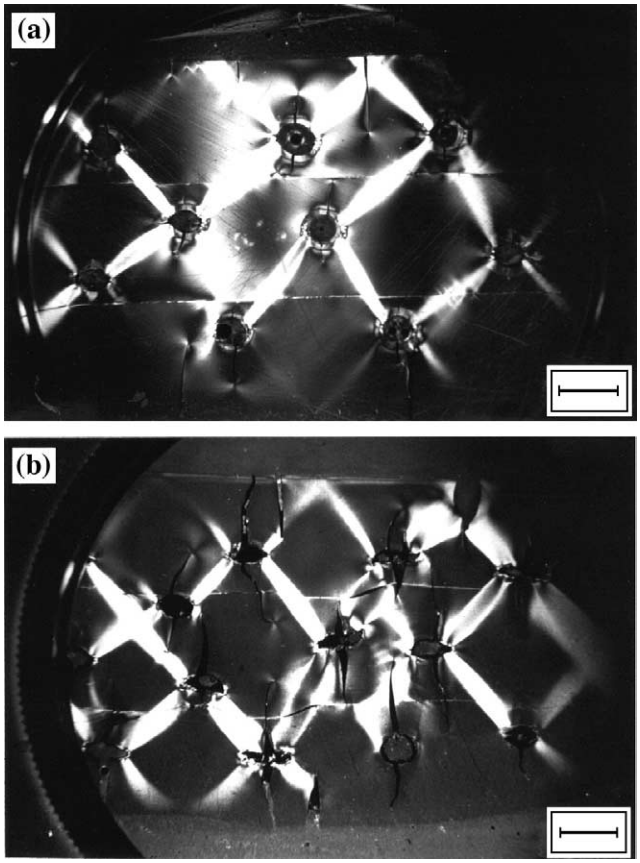

Fig. 6. (a) Development of shear zones in PMMA models containing multiple weak flaws in (a) low and (b) high concentrations. Permanent bulk shortening in the model was 4 and 6% in (a) and (b), respectively. Scale bar: 0.5 cm.

experimental modelling. Secondly, in multiple flaw models tensile cracks formed parallel to the bulk compression direction, which were preferentially located on either side of flaws. Some cracks also developed at the model boundary. These cracks appear to have developed at a later stage of deformation, as they cut across sharply shear zones. In places, the cracks show localisation of plastic strain at their tips, which is evident from birefringence zones.

3. Theoretical model

3.1. Mathematical derivation

Experimental observations described above indicate that a mechanically weak flaw induces plastic failure preferentially in its neighbourhood, developing shear zones In order to analyse this, we employ the plane theory of elasticity to derive the perturbed stress field around a flaw, and then simulate shear zones in the perturbed stress field by imposing Von Mise's yield criterion. Consider a circular flaw of radius a in an infinitely extended elastic medium with shear modulus μ_m. The material inside the flaw is also assumed to be elastic, but of different shear modulus, say μ_i. We again consider that the flaw is perfectly welded with the matrix, and there is no slip at their interface during the deformation. A Cartesian co-ordinate frame, xy is chosen at the centre of the flaw with the x axis parallel to the direction of bulk compression p (Fig. 7). The stress components at any point in the neighbourhood of the flaw can be expressed in terms of the polar co-ordinates as (Muskhelishvilli, 1953):

$$\sigma_{rr} = -\frac{p}{2}\left[1 - \gamma\frac{a^2}{r^2} + \left(1 - 2\beta\frac{a^2}{r^2} - 3\delta\frac{a^4}{r^4}\right)\cos 2\theta\right] \quad (1a)$$

$$\sigma_{\theta\theta} = -\frac{p}{2}\left[1 + \gamma\frac{a^2}{r^2} - \left(1 - 3\delta\frac{a^4}{r^4}\right)\cos 2\theta\right] \quad (1b)$$

$$\sigma_{r\theta} = \frac{p}{2}\left[1 + \beta\frac{a^2}{r^2} + 3\delta\frac{a^4}{r^4}\right]\sin 2\theta \quad (1c)$$

β, γ and δ are constants. They are functions of the rheological parameters and their expressions are as follows:

$$\beta = 2\frac{(\mu_m - \mu_i)}{\mu_m + \mu_i\chi_m}, \qquad \gamma = \frac{\mu_m(\chi_i - 1) - \mu_i(\chi_m - 1)}{2\mu_i + \mu_m(\chi_i - 1)}, \qquad \delta = -\frac{(\mu_m - \mu_i)}{\mu_m + \mu_i\chi_m} \quad (2)$$

where

$$\chi_m = \frac{\lambda_m + 3\mu_m}{\lambda_m + \mu_m}, \qquad \chi_i = \frac{\lambda_i + 3\mu_i}{\lambda_i + \mu_i} \quad (3)$$

λ_i and λ_m are the Lame's constants for the flaw and matrix, respectively. If the material inside the flaw is extremely weak compared with the matrix, it can be treated as a hole, and in that case $\mu_i = 0$ and it then follows that: $\beta = 2$, $\gamma = 1$, $\delta = -1$. However, the values of these constants will be different when μ_i is not zero. Now, the expressions of the functions in Eq. (2) become simple if both the flaw and the matrix are assumed to be incompressible, i.e. $\chi_m = \chi_i = 1$. The constants β, γ, and δ are then:

$$\beta = 2\frac{R-1}{R+1}, \qquad \gamma = 0, \qquad \delta = -\frac{R-1}{R+1}, \quad \text{where } R = \mu_m/\mu_i \quad (4)$$

In the following discussion we shall use the parameter R as a measure of competence contrast between the matrix and flaw.

The expressions of the stress functions (Eqs. (1a)–(1c)) can be rewritten into simple forms as:

$$\sigma_{rr} = -\frac{p}{2}\left[1 + \left(1 - 4K\frac{a^2}{r^2} + 3K\frac{a^4}{r^4}\right)\cos 2\theta\right] \quad (5a)$$

$$\sigma_{\theta\theta} = -\frac{p}{2}\left[1 - \left(1 + 3K\frac{a^4}{r^4}\right)\cos 2\theta\right] \quad (5b)$$

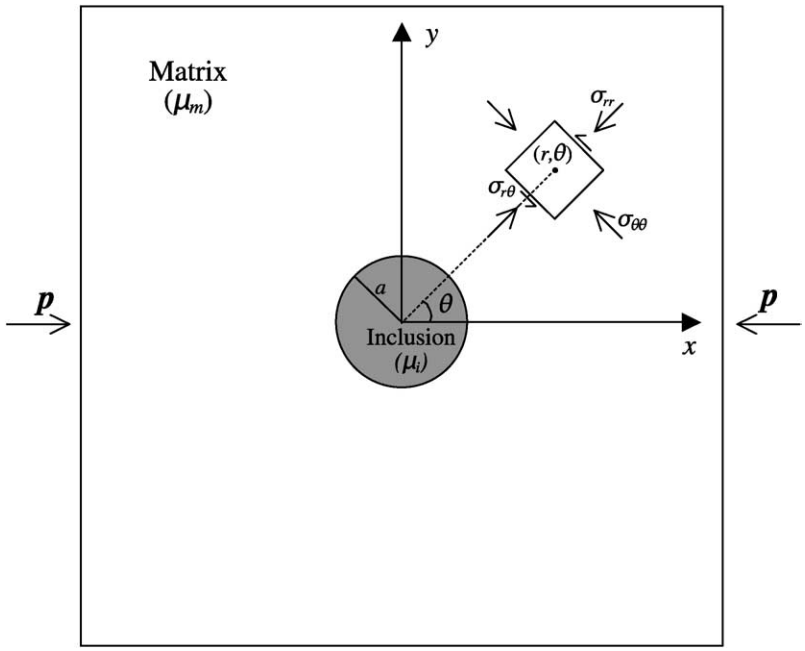

Fig. 7. Consideration of Cartesian co-ordinate system and presentation of stress components in polar co-ordinates. p is the far-field stress.

$$\sigma_{r\theta} = \frac{p}{2}\left[1 + 2K\frac{a^2}{r^2} - 3K\frac{a^4}{r^4}\right]\sin 2\theta \tag{5c}$$

where

$$K = \frac{R-1}{R+1}.$$

3.2. Numerical simulations of shear zones in single flaw models

With the help of Eqs (5a)–(5c) we can now simulate shear zones in the perturbed stress field around a flaw by imposing a yield criterion. According to the Von Mise's criterion (Jaeger, 1969), the condition for plastic failure in plane stress is as follows:

$$(\sigma_1 - \sigma_2)^2 + \sigma_1^2 + \sigma_2^2 = 2\sigma_0^2 \tag{6}$$

σ_1 and σ_2 are the principal stresses, and σ_0 is the yield strength of the matrix. Writing σ_1 and σ_2 in terms of σ_{rr}, $\sigma_{\theta\theta}$ and $\sigma_{r\theta}$, and substituting the derived expressions in Eq. (6), we have:

$$(\sigma_{rr} - \sigma_{\theta\theta})^2 + \left(\sigma_{rr}\sigma_{\theta\theta} + 3\sigma_{r\theta}^2\right) = \sigma_0^2 \tag{7}$$

The matrix yields plastically in the stress field around a flaw (Eqs. (5a)–(5c)), where Eq. (7) is satisfied. It is evident that the stress field around the flaw will depend on the rheological contrast parameter R, and the bulk compressive stress p, which in the foregoing analysis is expressed as σ^*, normalised to the yield strength of matrix σ_0.

We performed sets of numerical simulations by varying these two non-dimensional parameters: R and σ^*. The simulations were made with the help of a computer programme in Visual Basic, which involved the following steps. (1) A Cartesian space was considered, as stated earlier, and points at regular intervals were taken in a Cartesian grid. (2) The Cartesian co-ordinates of the points were then transformed into polar co-ordinates, as the theory presented above is in polar co-ordinates. (3) The space was subjected to a far-field stress p, the input of which in the computation was given by a value normalized to the yield strength of the matrix, chosen as an arbitrary number. (4) Using Eqs. (5a)–(5c) the stress components were determined and put in the left hand side of Eq. (7). (5) Finally, a stress factor (S_F) was determined considering the ratio of the values of the left- and right-side expressions in Eq. (7). (6) Points with $S_F > 1$ were plotted in the chosen space to simulate plastic zones in the numerical model.

A set of numerical models is presented, which were run by increasing the applied stress σ^* in successive steps. Fig. 8 shows the geometry of shear zones obtained at different bulk stresses. It was found that shear zones are not perceptible in the model till σ^* reaches a threshold value. For σ^* exceeding this value, the locales allowing plastic failure define small wedge-shaped zones located at the tips of the flattened flaws (Fig. 8). Within these regions the maximum stresses occur in circular domains, suggesting dominant plastic deformation localising in small domains at the tips of the flaw. At higher given bulk stress the plastic zones are obtained in the form of two conjugate tongues oriented at a low angle (20°) to the bulk compression direction and with a dihedral angle of 40°. When σ^* was increased to 0.9, the two tongues increase in area, defining elliptical shear zones in conjugate sets. They make higher

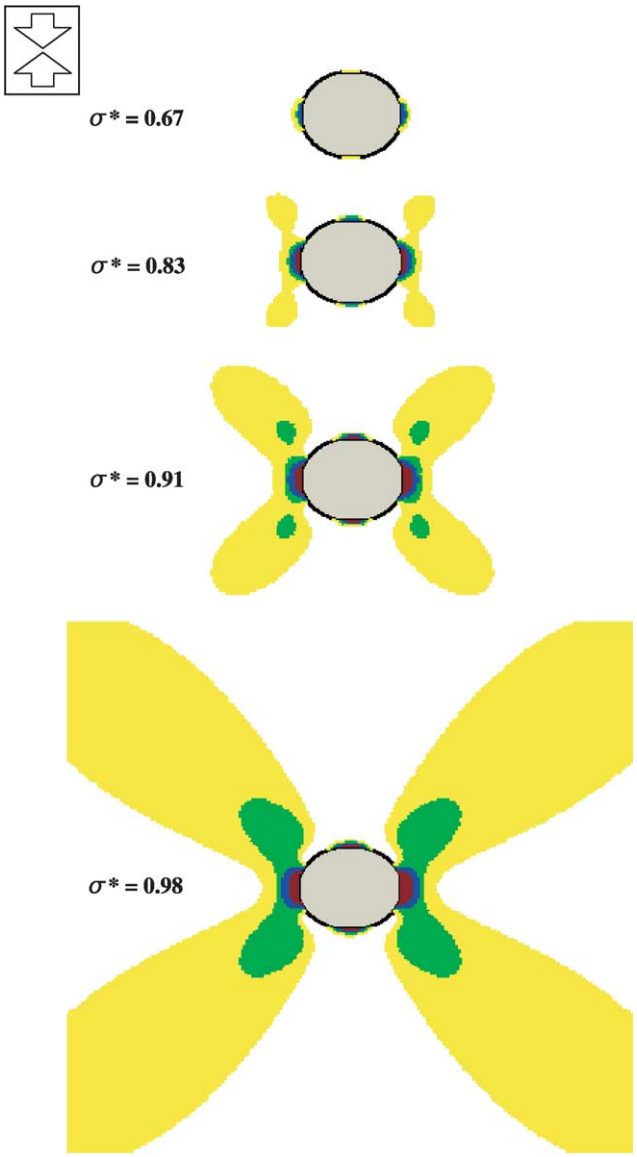

Fig. 8. Numerical simulations of shear zones around a mechanical flaw under different far-field stresses (σ^*), normalised to the yield strength of the matrix. Black to light grey shades successively represents the values of stress factor S_F greater than 2, 1.5, 1.25, and 1, respectively. See text for the expression of S_F. $R = 15$.

inclinations, about 46° to the bulk compression direction. With a further increase in σ^*, the plastic zones define elliptical zones with larger length to thickness ratios, and thereby give rise to the geometry of shear zones, as observed in physical experiments (Fig. 4b). The plastic zones show little variation in their orientations with further increase in bulk stress.

The principal findings from numerical simulations are: (1) weak flaws act as sites for nucleation of shear zones, (2) the zones in its rudimentary stage occur at a low angle to the bulk compression direction, but the angle increases with increase in the applied stress, and finally assumes a stable value, (3) the shear zones are typically tapered in geometry.

3.3. Controls of flaw–matrix competence contrast

We ran a set of numerical experiments by varying the competence contrast parameter R, keeping the applied stress σ^* constant The experiments reveal that a flaw does not induce plastic failure in its neighbourhood unless R attains a threshold value. We determined the threshold values of R for different applied stresses, and defined the conditions for plastic failure in the σ^*–R space.

The bulk stress required for nucleation of shear zones decreases nonlinearly with increasing shear modulus ratio between the matrix and flaw (Fig. 9). The decrease occurs steeply at low values of the ratio, whereas the stress varies gently at larger values of the ratio, and tends to assume an asymptotic value (about 0.5) when the ratio is very large (greater than 10). The calculation implies that a system containing mechanical flaws develops shear zones through plastic failure at a bulk stress less than the yield strength of the matrix. However, the stress must be at least half the yield strength, even if the flaw is extremely mechanically weak, being comparable with a hole in the system.

Another set of simulations was performed to study the orientation of shear zones as a function of R. The experiments reveal that the shear zones do not show any significant change in their orientation with increasing competence contrast (Fig. 10).

4. Discussion

Field observations suggest that rocks contain flaws, such as melt pockets, lenticular veins, isolated sericite bodies, which are weaker than the matrix and may be potential sites for nucleation of ductile shear zones (Grujic and Mancktelow, 1998). The development of flaw controlled shear zones has been demonstrated in finite element models based on elasto-viscous rheology (Mancktelow, 2002). In this study we have attempted to test in physical experiments how weak flaws in a system can actually control the formation of shear

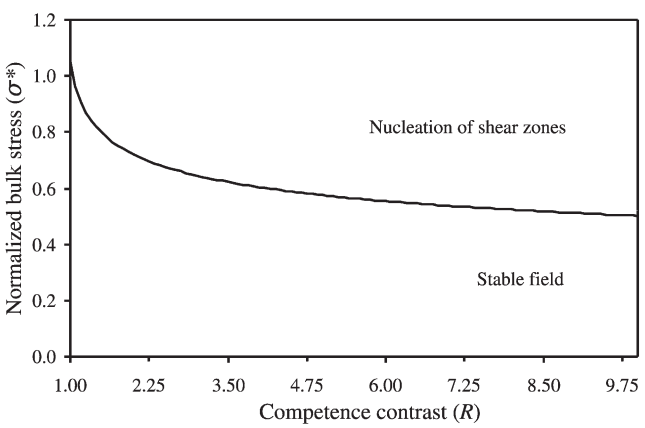

Fig. 9. Variation of the critical far-field stress required for nucleation of shear zones with the competence contrast between flaw and matrix.

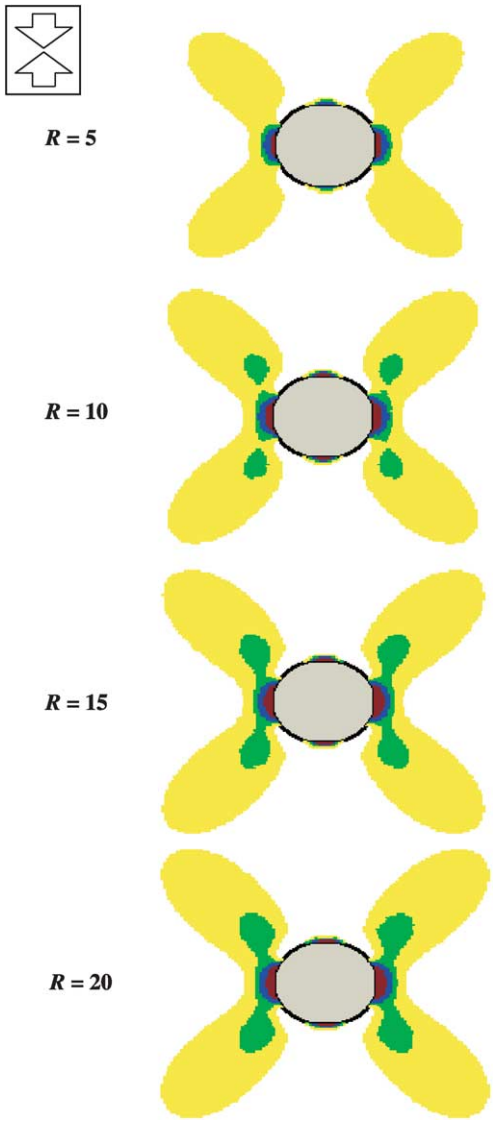

Fig. 10. Simulation of shear zones in numerical models for different values of the competence contrast parameter R under a constant far-field stress ($\sigma^* = 0.93$). Grey shades are used as in Fig. 8.

zones. The experimental results grossly match with the earlier findings, although our experimental models are based on elastic–plastic rheology.

We have applied the plane theory of elasticity in numerical simulations of shear zones around a circular flaw of contrasting shear modulus. This application is convenient as it involves simple, analytical solutions for the stress perturbation due to a circular flaw. The shear zone patterns in numerical models conform to those observed in physical experiments.

In physical experiments a single flaw in the model nucleate shear zones in the form of conjugate sets, where the individual zones are characteristically tapered in geometry, widening away from the flaw. The geometry is consistent with that obtained from numerical simulations based on the plane theory of elasticity. It thus appears that shear zones develop by plastic failure of the matrix material in response to the perturbed stress field in the neighbourhood of the weak flaw. In physical experiments they make an average angle of 42° to the bulk compression. However, the shear zones in numerical models are inclined at slightly higher angles. This difference is probably due to some differences in factors developed in physical and numerical experiments. We have modelled weak zone controlled shear zones considering the material isotropic before and after the plastic failure. On the contrary, the material might have acted mechanically anisotropic in the course of plastic deformation. Secondly, numerical simulations were developed considering the weak flaws ideally circular in cross-section, which may not be exactly so in physical experiments. There might be some departures in weak zone geometry from the theoretical consideration. The third probable reason may be attributed to the mechanical condition at the flaw–matrix interface. However, at this stage we cannot provide any concrete explanation for this small difference in shear zone orientations obtained from the theory and physical experiments.

Numerical experiments indicate that weak flaws can induce nucleation of shear zones only when the flaw–matrix competence contrast exceeds a threshold value. In geological settings weak zones may develop in rocks due to processes like partial melting or local fluid controlled softening. However, they will not induce localization of shear zones unless they become sufficiently softer than the bulk material. The system will deform developing a heterogeneous strain field around the weak zone, but not in the form of shear zones, as demonstrated in earlier (Mancktelow, 2002) and present models.

We have shown the conditions for nucleation of weak zone controlled shear zones in relation to two physical factors: (1) shear modulus ratio of flaw and matrix and (2) the ratio of applied bulk stress and the yield strength of matrix. The theoretical formulation is based on a single flaw system, considering the flaw occurring in an infinite elastic medium. The theoretical results are applicable to rocks containing flaws in low volume concentrations. In the approach flaw size does not appear to be a parameter, as the matrix is assumed to be of infinite extent. Recent studies show that flaws occurring in large volume concentrations mechanically may interact with one another, and thereby develop stress fields in the neighbourhood different from that of single, non-interacting flaws (Mandal et al., 2003; Samanta et al., 2003). The effect of such mutual interaction probably results in a variation of shear zone orientations in multiple flaw models, as noticed in our physical models. It thus appears that in multiple flaw systems the flaw size will be an additional physical parameter in controlling shear zone nucleation, as it determines the matrix/flaw volume ratio. In that case, the bulk stress required for nucleation of shear zones would be different from that derived from the theory based on single flaw systems presented in this paper.

Some of the features observed in physical experiments have developed essentially due to our experimental

conditions. For example, minor shear zones formed where the flaw-controlled shear zones propagated to a large extent and met the model boundary. These minor shear zones would not have formed if the model were considered to be of infinite extent, as in the case of numerical models. However, this type of situation may occur in layered rock systems, where the layer interface can be potential locales for nucleation of subsidiary shear zones.

In multiple flaw models we induced flaws randomly in the model so that the shear zones would not grow tracking the initial flaw arrangement. However, it was observed in deformed models that shear zones nucleating at individual flaws coalesce along a preferential direction forming longer shear zones. Statistically, random flaws are likely to form rows of random orientations. Our experiments suggest that the coalescence of shear zones will be effective along rows of flaws of particular orientation, giving rise to shear zones showing preferred orientation with the compression direction, as often observed in naturally deformed rocks and numerical models (Mancktelow, 2002). Shear zone orientations are likely to show some variations maintaining a statistically defined dominant direction. Further studies are required to investigate how much the variation of orientation is sensitive to the initial concentration of flaws in the system.

5. Conclusions

The principal outcomes of our study are concluded along the following points:

1. Physical experiments on elastic–plastic models confirm earlier findings that weak flaws in rock systems can trigger nucleation of shear zones. Single flaws develop shear zones with the length dimension much larger than the flaw dimension. Thus, the presence of a mechanical flaw even incipient in size can lead to formation of strain localization in the form of shear zones.
2. In multiple flaw systems, minor shear zones around individual flaws coalesce with one another forming longer, through-going shear zones. The process of coalescence is more effective for flaws forming an array of favourable orientations. The through-going shear zones develop in well-defined conjugate sets when the flaw concentration is relatively high.
3. Numerical models based on the plane theory of elasticity show development of shear zones in a pattern resembling that observed in the physical experiments. It appears that shear zones can form through plastic failure of the matrix under the heterogeneous stress field around a weak mechanical flaw. This can happen under bulk stresses below the yield strength of the system considered to be homogeneous.
4. The bulk stress required for nucleation of shear zones decreases non-linearly with increasing matrix/flaw competence contrast, and tends to assume an asymptotic value when the contrast is very large. The calculation suggests that the bulk stress must be at least half the yield strength of the matrix for the nucleation of shear zones around a weak flaw, comparable with a hole.

Acknowledgements

We thank two anonymous reviewers for their detailed comments that greatly contributed to the improvement of the paper. We also thank Prof. C.W. Passchier for providing an outline in revising the manuscript. The Department of Science and Technology, India has provided financial support in carrying this work. Jadavpur University is gratefully acknowledged for extending a research fellowship to SM.

Appendix A

Numerical simulations presented in Section 3.2 involve functions describing the displacement in the matrix for a given bulk compression. Considering the matrix to be incompressible, the displacement at a point in the neighbourhood of a flaw can be expressed in terms of complex functions as:

$$2\mu(u+iv) = \varphi(z) - z\overline{\varphi'(z)} - \overline{\psi(z)} \tag{A1}$$

where u and v are the displacement components along the x and y co-ordinate axes respectively, and $\varphi(z)$ and $\psi(z)$ are complex functions, and the prime and bar represent the first derivative and conjugate of the functions, respectively (Muskhelishvilli, 1953). For the present case, their expressions follow:

$$\varphi(z) = \frac{p}{4}\left(z + \frac{\beta R^2}{z}\right) \tag{A2a}$$

$$\psi(z) = -\frac{p}{2}\left(z + \frac{\gamma R^2 z}{z} + \frac{\delta R^4}{z^3}\right) \tag{A2b}$$

Differentiating Eq. (A2a), we have:

$$\varphi'(z) = \frac{p}{4}\left(1 - \frac{\beta R^2}{z^2}\right) \tag{A3}$$

Replacing $z = re^{i\theta}$ in Eqs. (A2a), (A2b) and (A3), and substituting their derivative expressions in Eq. (A1) and

finally separating the real and imaginary parts, we get:

$$u = \frac{p}{8r\mu}\left[\beta R^2\left(2\cos^3\theta - \sin 2\theta \sin\theta\right) + 2\cos\theta\left(r^2 + \gamma R^2\right) + \frac{2\delta R^4}{r^2}\cos 3\theta\right] \tag{A4a}$$

$$v = \frac{p}{8r\mu}\left[-\beta R^2\left(2\sin^3\theta - \sin 2\theta \cos\theta\right) - 2\sin\theta\left(r^2 - \gamma R^2\right) + \frac{2\delta R^4}{r^2}\sin 3\theta\right] \tag{A4b}$$

After putting the values of the constants β, γ and δ (Eq. (4)), the above equations simplify as:

$$u = \frac{p}{8r\mu}\left[2KR^2\left(2\cos^3\theta - \sin 2\theta \sin\theta\right) + 2r^2\cos\theta + \frac{2KR^4}{r^2}\cos 3\theta\right] \tag{A5a}$$

$$v = \frac{p}{8r\mu}\left[-2KR^2\left(2\sin^3\theta - \sin 2\theta \cos\theta\right) - 2r^2\sin\theta - \frac{2KR^4}{r^2}\sin 3\theta\right] \tag{A5b}$$

References

Anand, L., Spitzig, W.A., 1980. Initiation of localised shear bands in plane strain. Journal of Mechanics and Physics of Solids 28, 113–128.

Bjornerud, M.G., Zhang, H., 1995. Flow mixing inclusion matrix coherent mantle growth and the development of porphyroclast tails. Journal of Structural Geology 17, 1347–1350.

Bowden, P.B., Raha, S., 1970. The formation of micro-shear bands in polystyrene and polymethylmethaacrylate. Philosophical Magazine 22, 463–482.

Christiansen, P.P., Pollard, D.D., 1997. Nucleation, growth and structural development of mylonitic shear zones in granitic rocks. Journal of Structural Geology 19, 1159–1172.

Cobbold, P.R., 1977. Description and origin of banded deformation structures. I. Regional strain, local perturbations, and deformation bands. Canadian Journal of Earth Sciences 14, 1721–1731.

ten Grotenhuis, S.M., Passichier, C.W., Bons, P.D., 2002. The influence of strain localisation on the rotation behaviour of rigid objects in experimental shear zones. Journal of Structural Geology 24, 485–499.

Grujic, D., Mancktelow, N.S., 1998. Melt-bearing shear zones: analogue experiments and comparison with examples from southern Madagascar. Journal of Structural Geology 20, 673–680.

Hill, R., Hutchison, J.W., 1975. Bifurcation phenomenon in the plane tension test. Journal of Mechanics and Physics of Solids 23, 239–264.

Ildefonse, B., Mancktelow, N.S., 1993. Deformation around rigid particle: influence of slip at the particle/matrix interface. Tectonophysics 221, 345–359.

Jaeger, J.C., 1969. Elasticity, Fracture and Flow. Methuen, London, 268pp.

Jezek, J., Saic, S., Segeth, K., Schulmann, K., 1999. Three-dimensional hydrodynamical modelling of viscous flow around a rotating ellipsoidal inclusion. Computer and Geosciences 25, 547–558.

Kenkmann, T., Dresen, G., 1998. Stress gradients around porphyroclasts: palaeopiezometric estimates and numerical modelling. Journal of Structural Geology 20, 163–173.

Mair, K., Main, I., Elphick, S., 2000. Sequential growth of deformation bands in the laboratory. Journal of Structural Geology 22, 25–42.

Mancktelow, N.S., 2002. Finite-element modelling of shear zone development in viscoelastic materials and its implications for localisation of partial melting. Journal of Structural Geology 24, 1045–1053.

Mandal, N., Khan, D., Deb, S.K., 1992. An experimental approach to wide-necked pinch-and-swell structures. Journal of Structural Geology 14, 395–403.

Mandal, N., Samanta, S.K., Chakraborty, C., 2001. Numerical modelling of heterogeneous flow fields around rigid objects with spherical reference to particle paths, strain shadows and foliation drag. Tectonophysics 330, 177–194.

Mandal, N., Samanta, S.K., Bhattacharyya, G., Chakraborty, C., 2003. Deformation of ductile inclusions in a multiple inclusion system in pure shear. Journal of Structural Geology 25, 1359–1370.

Masuda, T., Ando, S., 1988. Viscous flow around a rigid spherical body: a hydrodynamical approach. Tectonophysics 148, 337–346.

Muskhelishvilli, N.I., 1953. Some Basic Problems of the Mathematical Theory of Elasticity. Noordhoff, Groningen, Holland, 704pp.

Passchier, C.W., 1994. Mixing in flow perturbations: a model for development of mantle porphyroclasts in mylonites. Journal of Structural Geology 16, 733–736.

Pennacchioni, G.P., Fasolo, L., Cecchi, M.M., Salasnich, L., 2000. Finite-element modelling of simple shear flow in Newtonian and non-Newtonian fluids around circular rigid particle. Journal of Structural Geology 22, 683–692.

Porier, J.P., 1980. Shear localization and shear instability in materials in the ductile field. Journal of Structural Geology 2, 135–142.

Ramsay, J.G., Lisle, R., 2000. The Techniques of Modern Structural Geology. Vol. 3. Application of Continuum Mechanics in Structural Geology. Academic Press, London.

Samanta, S.K., Mandal, N., Chakraborty, C., 2003. Flow patterns around rigid inclusions in a multiple inclusion system undergoing bulk simple shear deformation. Journal of Structural Geology 25, 209–221.

Segall, P., Simpson, C., 1986. Nucleation of ductile shear zones on dilatant fractures. Geology 14, 56–59.

Treagus, S.H., Lan, L., 2000. Pure shear deformation of square objects, and applications to geological strain analysis. Journal of Structural Geology 22, 105–122.

Tvergaard, V., Needleman, A., Lo, K.K., 1981. Flow localization in the plane strain tensile test. Journal of Mechanics and Physics of Solids 29, 115–142.